J. Water Environ. Nanotechnol., 8(4): 320-333 Autumn 2023

ORIGINAL RESEARCH PAPER

Optimization of COD removal of raw landfill leachate using the magnetic graphene oxide/WO_3 nanocomposite: Isotherms, kinetics, and thermodynamics studies

Zahra Mirkazehi[1], Mohammad Reza Rezaei[1], Mohammad Hossein Sayadi [1,2]*

[1] *Department of Environmental Engineering, Faculty of Natural Resources and Environment, University of Birjand, Birjand, Iran*
[2] *Faculty of Natural Resources and Environment, Shahid Bahonar University of Kerman, Kerman, Iran*

Received: 2023-05-24 Accepted: 2023-08-16 Published: 2023-10-11

ABSTRACT
Landfill leachate is the fluid percolating through the landfill and is one of the most important environmental challenges that lead to the contamination of water and soil resources. In this study, magnetic graphene oxide nanoparticles with WO_3 (GO-Fe_3O_4/WO_3) were synthesized through the hydrothermal method to eliminate chemical oxygen demand (COD) from leachate. The obtained products were characterized using X-ray diffraction (XRD), Fourier Transform Infrared Spectroscopy (FTIR), Scanning Electron Microscopy (SEM), Thermogravimetric analysis (TGA), and Vibrating sample magnetometer (VSM) analysis. The influence of various operating parameters, such as initial solution pH, adsorbent dosage, contact time, and temperature, on COD removal was studied. Additionally, kinetic, isotherm and thermodynamic studies were conducted to evaluate the adsorption capacity of the adsorbent. The results revealed that the maximum adsorption capacity of GO-Fe_3O_4/WO_3 was 2500 mg/g adsorbent at pH 4, a contact time of 90 minutes, an adsorbent dosage of 25 mg g^{-1}, and a temperature below 298 K, respectively. According to the adsorption kinetic fitting results, the experimental adsorption data were well described by the pseudo-second-order kinetic with an R^2 value of 0.97, and the Freundlich isotherm equation with an R^2 value of 0.99. The thermodynamic results indicated that the adsorption was spontaneous and exothermic for COD adsorption. In general, the adsorption process of the synthesized GO-Fe_3O_4/WO_3 nanocomposite revealed that it is highly effective for landfill leachate treatment and has great practical value in leachate treatment.

Keywords: *Adsorption isotherms; COD; GO-Fe_3O_4/WO_3; Kinetic; Landfill leachate*

How to cite this article
Mirkazehi Z., Rezaei M., Sayadi M., Optimization of COD removal of raw landfill leachate using the magnetic graphene oxide/WO_3 nanocomposite: Isotherms, kinetics, and thermodynamics studies. J. Water Environ. Nanotechnol., 2023; 8(4): 320-333.
DOI: 10.22090/jwent.2023.04.001

INTRODUCTION

Production of landfill leachate is one of the most important environmental challenges that lead to surface water groundwater and soil contamination [1]. Landfill leachate is a very strong odor and dark brown liquid, which is caused by the decomposition of the organic part of the waste as a result of physicochemical and biological processes in combination with rainwater [2]. Its characteristics vary according to the amount and type of waste produced, microbial population, the degree of stabilization of the hydrological structure of the landfill, climatic conditions and exploitation,

* Corresponding Authors Email: *mrrezaei@birjand.ac.ir*

This work is licensed under the Creative Commons Attribution 4.0 International License.
To view a copy of this license, visit http://creativecommons.org/licenses/by/4.0/.

as well as the age and stages of decomposition [3]. In case of not collecting and treating the leachate from the municipal solid waste landfill is a serious contamination threat to public health and the environment [4]. Leachate is a type of liquid that is released from a landfill site and can contain both dissolved and suspended matter, including organic materials [5]. The measure of chemical oxygen demand (COD) is used to determine the amount of oxygen needed to chemically oxidize any organic compounds present in water or other liquid samples [6]. When there is an increase in COD levels within leachate, this indicates a high concentration of organic pollutants that could potentially cause harm to both the environment and human health if not managed and treated appropriately [7].

In recent years, techniques including biological methods and chemical and physical processes have been used to treat and reduce the pollution load of leachate [8]. The adsorption process is currently considered the most frequently used technology for removing environmental pollution due to its simple operation, low cost, friendly approach, and perfect remediation effect. Adsorbents such as metal oxides, clay minerals, carbon nanotubes, and biological adsorbents have been utilized for the removal of pollutants from aqueous solutions [9]. Therefore, these materials don't have wide-spread used high adsorption performance, which is due to the limited number and type of containing oxygen functional groups [10]. However, the synthesis of novel adsorbents with chemical stability and high adsorption capacity attracts more attention [11].

Graphene oxide (GO), a unique material, as a newly developing carbon nanomaterial and the interesting properties of graphene, has a separate sheet structure with a variety of oxygen-containing functional groups on its edges and surfaces [12]. Graphene oxide has attracted considerable attention from researchers due to its fascinating properties such as high flexibility, high surface area, good chemical stability, chemical inertness, high electrical conductivity, light transmission, excellent hydrophobicity, and adsorption of some metal ions at the nanoscale [13]. The presence of oxide groups on the surface of graphene helps to make it usable for a wide range of applications by performing chemical modifications [14]. Among the capabilities of graphene oxide is its high adsorption capacity for metal ions and organic pollutants from aqueous solutions [15]. At the same time, magnetizing this material helps in high adsorption and easy separation from solution environments by magnets [16]. For this purpose, one suitable nanoparticle is magnetite (Fe_3O_4) nanoparticles which have been widely applied due to their biocompatibility, superparamagnetic properties, chemical stability, high saturation magnetization, and innocuousness [17, 18]. In recent years, Tungsten trioxide (WO_3) has been widely utilized for the elimination of organic contaminants from aqueous systems due to their environmentally benign and excellent adsorption [19, 20]. Tungsten trioxide (WO_3) is a chemical substance that is utilized as an adsorbent and nanocatalyst to eliminate pollutants from water systems. This material possesses unique properties that render it suitable for pollutant removal processes [21]. As an adsorbent, tungsten trioxide exhibits a high capacity to absorb organic pollutants from water. By forming chemical compounds with the pollutants, the pollutant molecules become attached to the surface of tungsten trioxide and separate from the solution. This absorption process can occur through physical or chemical means, establishing a connection between tungsten trioxide and the pollutant [22]. Further, tungsten trioxide functions as a nanocatalyst. Consequently, it can accelerate chemical processes and enhance the efficiency of pollutant removal. Upon contact with the tungsten trioxide surface, chemical reactions such as oxidation, hydrolysis, or corrosion may take place. These chemical activities facilitate the decomposition and destruction of pollutants, thereby increasing the efficacy of their removal [23]. Utilizing tungsten trioxide (WO_3) for the elimination of organic pollutants from water systems offers significant advantages. This material is both safe and environmentally friendly, capable of effectively removing a wide array of pollutants including water-soluble organic pollutants, dyes, odors, and heavy organic matter. Moreover, tungsten trioxide possesses recyclability and recoverability, enabling its reuse as an adsorbent in continuous processes [24]. In a recent study, Bankole et al. (2017) examined the potential of purified and polymer-functionalized carbon nanotubes (CNTs) as nanosorbents for the removal of chemically required oxygen (COD) from wastewater generated by the electroplating industry. They conducted batch adsorption experiments to evaluate the effectiveness of CNTs in this process [25]. In another study by Gholami et al. (2019) conducted a study where they utilized a nanocomposite known as magnetic graphene

oxide-polydopamine oxide (M-GO-PDA) to eliminate chemical oxygen demand (COD) from aqueous solutions[26] . Lam et al. (2020) employed a Z-plan structure consisting of an anodic WO_3 nanocatalyst loaded onto hexagonal rods of ZnO/Zn (WO_3/ZnO/Zn) for the purpose of removing COD from aqueous solutions [27].

In the present work, magnetic graphene oxide nanoparticles synthesized with WO_3 (GO-Fe_3O_4/WO_3) were prepared using the hydrothermal method. The synthesized nanocomposite was utilized for the removal of chemical oxygen demand (COD) from leachate. The physicochemical properties of the prepared nanocomposite were investigated using techniques such as XRD, FT-IR, FE-SEM, TGA, and VSM. The effects of various factors, including the pH of the solution, contact time, adsorbent dosage, and temperature on the adsorption process, were studied. Furthermore, kinetic, isotherm, and thermodynamic models were employed to analyze the removal mechanisms and describe the physicochemical properties of the material.

EXPERIMENTAL

Materials

Graphite powder, sulphuric acid (96%), sodium nitrate (99%), hydrogen peroxide (30%), hydrochloric acid (37%), potassium permanganate ($KMnO_4$), ammonium nitrate ($KMnO_4$), $FeCl_2.4H_2O$, $FeCl_3.6H_2O$, tungsten hexachloride (WCl6), polyethylene glycol (PEG), sodium oxidative (NaOH), ammonia (25%), ethanol (99%,) were purchased from Merck Co, Germany.

Graphene oxide (GO)

Graphene oxide (GO) was successfully synthesized from graphite powder using the modified Hummer's method [28]. In brief, 3 g of graphite powder and 2 g of NH_4NO_3 were added to 60 ml of 98% H_2SO_4 with stirring in an ice bath for 50 min. After that, 15 g of $KMnO_4$ was slowly added to the mixture and continued stirring for one hour until the mixture's dark green color appeared, and then placed in a water bath at 45 °C. The mixture was stirred for one hour to form a thick paste. Next, 150 mL of double-deionized H_2O was added to this formed paste with stirred at 90 °C for one hour until a brown color formed. The mixture was diluted with 100 mL of deionized water, and then 30 mL of 30% hydrogen peroxide (H_2O_2) was slowly added, while the color of the mixture turned yellow after the addition of H_2O_2. Finally, the product was filtered and washed with 5% HCl aqueous solution to remove metal ions followed with deionized water several times until the pH of 7. The obtained graphene oxide was dried in a vacuum oven at 60 ◦C for 24 h.

Synthesis of GO-Fe_3O_4 nanoparticles

The synthesis of magnetic nanoparticles (GO-Fe_3O_4) was produced using the ex-situ co-precipitation method [29]. At first, 50 mg of GO was dispersed in 100 mL of deionized water via sonication for one hour to obtain a homogeneous solution and then added to the mixed solution of $FeCl_2.4H_2O$ (0.064 M) and $FeCl_3.6H_2O$ (0.129 M) with stirring for one hour. The solution was maintained at pH 10 by adding 1 M NaOH after 1 h of stirring. Next, the resultant mixture was stirred for one hour at 150°C. Finally, the GO-Fe_3O_4 magnetic nanoparticles were separated by an external magnet and washed several times with distilled water and ethanol, and then dried in a vacuum oven at 60 °C for 24 hours.

Synthesis of GO-Fe_3O_4/WS_2 nanocomposite

Synthesis of WO_3 nanoparticles was done by hydrothermal method [30]. In the first step, 1.5 mmol of WCl6 and 0.3 g of PEG were added to 70 ml of ethanol solution and dispersed by ultrasonication for 30 min. After that, the prepared mixture was placed in an autoclave at 110 °C for 4 hours. The obtained nanoparticles were separated by an external magnet washed several times with deionized water and then dried in a vacuum oven at 60°C for 12 hours.

To prepare the graphene oxide magnetic nanocomposite reinforced with tungsten oxide: First, the graphene oxide magnetic nanocomposite was dispersed in 10 ml of deionized water and placed in an ice bath under vigorous stirring for 10 min. Afterward, the WO_3 was mixed with the solution and stirred for one hour within an ice bath, then the product was kept at 0-4 °C for 120 min. Finally, the obtained product was separated by an external magnet washed several times with distilled water and ethanol, and dried in a vacuum oven at 60°C for 8 hours. The preparation process of synthesizing the GO-Fe_3O_4/WO_3 nanocomposite is shown in Fig. 1.

Characterization techniques

The characteristics of the surface structure and

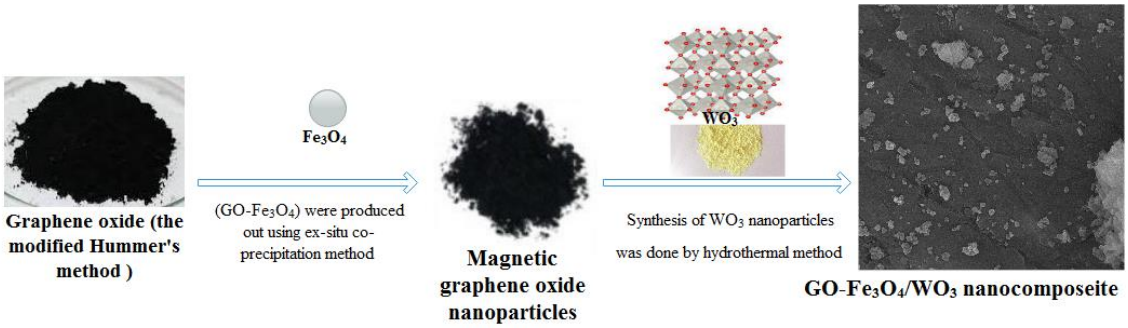

Fig. 1. The preparation process of synthesizing the GO-Fe_3O_4/WO_3 nanocomposite.

Table 1. Physicochemical characteristics of raw leachate

Parameters	Values
pH	7.12
BOD_5 (mg/L)	7520
COD (mg/L)	12580
Cl (mg/L)	4128.5
NO_3^- (mg/L)	8.34
PO_4^{-2} (mg/L)	14.7
TP (mg/L)	13.1
TSS (mg/L)	430

morphology of the samples were observed using a field emission scanning electron microscope (FESEM, ZEISS-SUPRA55, Germany). The X-ray diffraction (XRD) patterns were determined by Shimadzu 6000 diffractometer using Cu-Kα radiation (λ¼1.54056Å). Fourier transform infrared (FT-IR) was recorded by Nicoletis 10, Thermo Scientific (Waltham, MA, USA) with the KBr pellets over the range of 400-4000 cm^{-1}. The samples prepared by thermogravimetric analysis (TGA) were performed STA449C Jupiter (Netzsch) instrument in a nitrogen atmosphere at a rate of 20 °C/min. Magnetic hysteresis of the synthesized nanoparticles was measured by using a vibrating sample magnetometer (VSM) Qunantumpesign, MPMS3, USA.

Adsorption experiments

The batch adsorption experiments were carried out in a set of Erlenmeyer flasks (250 mL) using different weights of produced adsorbent mixed with 100 ml leachate solution at room temperature (25 ± 1°C). After completion of the adsorption process, the solid sorbent was separated from the sample solution by a magnetic field, and the concentration of COD was determined using a spectroscopy method based on the oxidation of the organic matter by potassium dichromate ($K_2Cr_2O_7$), where the effect of solution pH, contact time, adsorbent dose, and temperature was investigated. The physical and chemical characteristics of the tested leachate are presented in Table 1.

The adsorption removal and uptake capacity were determined by using the following presented Eqs. (1) and (2): [31]

$$R(\%) = \frac{C_i - C_t}{C_i} \times 100 \quad (1)$$

$$q_e = \frac{V\,(C_i - C_e)}{m} \quad (2)$$

Where C_i and C_t are the initial concentration of COD at time (0 and t) resolution (mg L^{-1}), respectively, qe is the adsorption capacity in (mg g^{-1}), the total removal efficiency (R%) is the value of COD adsorbed by the adsorbent, Ce (mg L^{-1}) is the equilibrium concentration of the COD in solution, V is the volume of used solution (L) and m is the mass of the adsorbent in (g).

Characteristics of studied leachate

Equilibrium Adsorption Kinetics

In this study, pseudo-first-order (PFO), pseudo-second-order (PSO), and intraparticle kinetic

models were used to evaluate the adsorption process. The three models fitting formulas are as follows: [32, 33]

$$\log(q_e - q_t) = \log q_e - k_1 t \quad (3)$$

$$\frac{t}{q_t} = \frac{1}{k_2 q_e^2} + \frac{1}{q_e} \quad (4)$$

$$Q_t = k_{id} t^{0.5} + c_i \quad (5)$$

Where q_t is at time t (mg g^{-1}) and q_e is the amounts of COD adsorbed in mg g^{-1} at equilibrium, k_1 is the rate constant for the PFO adsorption process (min^{-1}) and K_2 is the kinetic rate constant for the PSO adsorption process (g/mg/min), respectively. d_C/d_t represents the rate of change of the concentration (C) of a species within the particle to time (t). f(C) is a function that describes the dependence of the reaction rate on the concentration.

Equilibrium Adsorption Isotherm

The surface adsorption isotherm is based on the hypothesis that the adsorption process takes place all over the adsorbent and is independent of the occupied surfaces. Isotherm models reveal the relationship between metal ion concentrations in solution and the amount of ion adsorbed on a specific adsorbent at a constant temperature. To determine the adsorption capacity of magnetic nano absorbent to remove COD leachate, the nonlinear form of Langmuir (Equation 5), Freundlich (Equation 6), and Dubinin-Radushkevich (Equation 6) models were studied, which can be described as follows [34, 35]:

$$q_e = \frac{q_m K_L C_e}{1 + K_L C_e} \quad (6)$$

$$q_e = K_f C_e^{1/n} \quad (7)$$

$$qe = q_s \exp^{(-K_{ad}\varepsilon^2)} \quad (8)$$

The separation factor (RL) helps to prove whether the adsorption process is favorable or unfavorable and it was expressed as equation 8:

$$R_L = 1/1 + K_L Co \quad (9)$$

Where q_e (mg/g) and C_e (L/mg) are the adsorption capacity at equilibrium and the equilibrium concentration of adsorbate, respectively. C_0 (L/mg) is the initial mercury concentration, q_m (mg/g) is the maximum adsorption capacity to form a complete monolayer, and K_L (L mg^{-1}), K_F ((mg/g) $(L/mg)^{1/n}$), K_F is isotherm constant indicates the capacity parameter (mg/g) (L/mg)1/n, n is the dimensionless exponent of the Freundlich equation. q_s is the maximum adsorption capacity, K_{ad} is the free energy of adsorption per mole of adsorbate (mol^2/J^2), and ε Polanyi potential is calculated using this equation: ε = RT. ln (1 + (1/C_e)); where R is the universal gas constant (8.314 J/mol. K), T is the temperature in Kelvin (K) and E the mean adsorption energy that is calculated using this equation: $E = 1/\sqrt{2K_{ad}}$.

RESULTS AND DISCUSSION

The X-ray diffraction (XRD)

Fig. 2a shows the XRD spectrum of the crystalline structure of GO, GO-Fe_3O_4, and GO-Fe_3O_4/WO_3 nanoparticles. As can be seen, the XRD spectrum of GO exhibits two strong peaks at 2h = 10.6 corresponding to the (002) plane [36]. The characteristic peaks of Fe_3O_4 appeared at the angles of 2θ = 27.46°, 35.63°, 43.14°, 57.40° and 62.97°, these are the corresponding crystalline planes (220), (311), (400), (422), (511) and (440) which verifies the crystal structure of Fe_3O_4 cubic spinel (JCPDS file no: 019-0629) [28]. The major diffraction peaks at 2θ values of 16.3°, 19.2° (011), 23.5° (120), 25.7° (111), 35.2° and 78.4° corresponding to (020), (011), (120), (111), (131) and (313) crystal planes, respectively, which are similar to the pattern referring to the presence of crystalline WO_3 (JCPDS file number: 84-886) [37]. The XRD pattern of the GO-Fe_3O_4/WO_3 composite indicates no characteristic diffraction peaks corresponding to the graphene oxide because of the disorders that occur in graphene oxide stacking during the composite formation, concurring with the earlier reports [38].

Fourier transform infrared (FT-IR)

The FT-IR spectra of typical vibration peaks of GO, GO-Fe_3O_4 , and GO-Fe_3O_4/WO_3 nanoparticles are shown in Fig. 2b. In the FT-IR spectrum of GO, the bands at 1624 cm^{-1}, 1450 cm^{-1}, and 1078 cm^{-1} were assigned to the bending and of aromatic C=C double bond, C-OH stretching bond, and stretching vibration of C-O bond, respectively [28, 39]. The existence of these peaks indicates that graphene oxide nanosheets with abundant oxygen functional

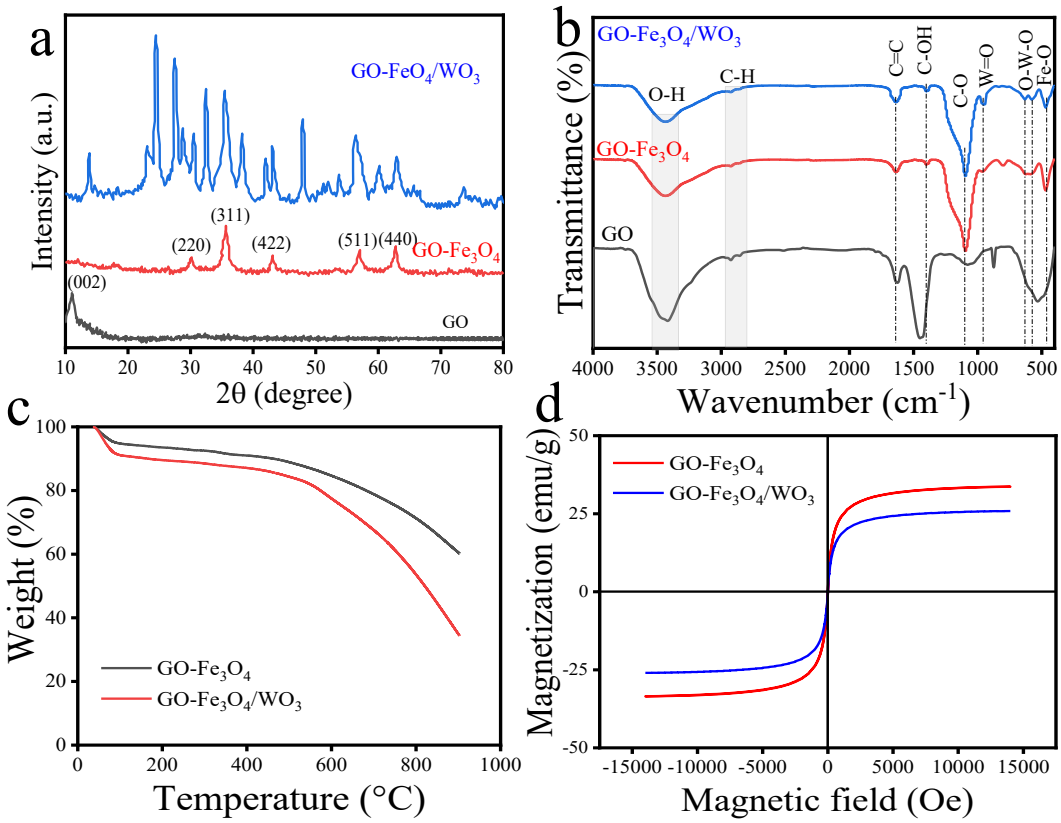

Fig. 2. (a) The XRD pattern, (b) Spectrum of FTIR, (c) TGA weight loss curves, (d) Magnetization curves of magnetic of GO-Fe_3O_4/WO_3 nanocomposite.

groups have been successfully synthesized. The broad band is observed at about 3400 cm^{-1} - 3500 cm^{-1}, which is related to the stretching vibration of O-H [40]. In the FT-IR spectra of magnetite-graphene oxide nanocomposite, the intense peak at 572 cm^{-1} is assigned to Fe-O stretching which displays high magnetite loaded in the prepared magnetite-graphene oxide nanocomposite [31, 41]. In the case of WO_3, broad absorption bands in the range 500-900 cm-1 are characteristic of the different O-W-O stretching vibrations of the monoclinic WO_3 crystal lattice [42].

Thermogravimetric analysis (TGA)

In Fig. 2c, the thermal behavior curves of GO-Fe_3O_4 and GO-Fe_3O_4/WO_3 nanoparticles were investigated. The mass loss for GO-Fe_3O_4 is approximately 6.45% at temperatures ranging from 26 to 110 degrees Celsius, which is attributed to the desorption of physically absorbed H_2O and the decomposition of oxygen-containing functional groups on the surface of GO-Fe_3O_4 [43]. The second weight loss occurs in the temperature range of 150-500 degrees Celsius and is about 2.15%, which could be related to the decomposition of remaining organic residues on the nanoparticles [44]. As observed in the TGA thermogram of the GO-Fe_3O_4/WO_3 nanocomposite, three weight reduction stages occur between 27 and 800 degrees Celsius. In the first stage, a weight loss of approximately 11.06% takes place at temperatures from 26 to 120 degrees Celsius, which is attributed to the removal of adsorbed water molecules and physically absorbed species. The weight reduction in the second and third stages, at temperatures of 150-550 degrees Celsius (3.7%) and 550-900 degrees Celsius (45.20%), respectively, can be attributed to the decomposition of organic and mineral residues in GO-Fe_3O_4/WO_3.

Vibrating sample magnetometer (VSM)

The magnetization curves of GO-Fe_3O_4 and GO-Fe_3O_4/WO_3 nanocomposites are shown in Fig. 2d. It can be seen that the saturation magnetization value of GO-Fe_3O_4 is approximately 35.7 $emug^{-1}$ at 15000 Oe, which could be due to the disruption

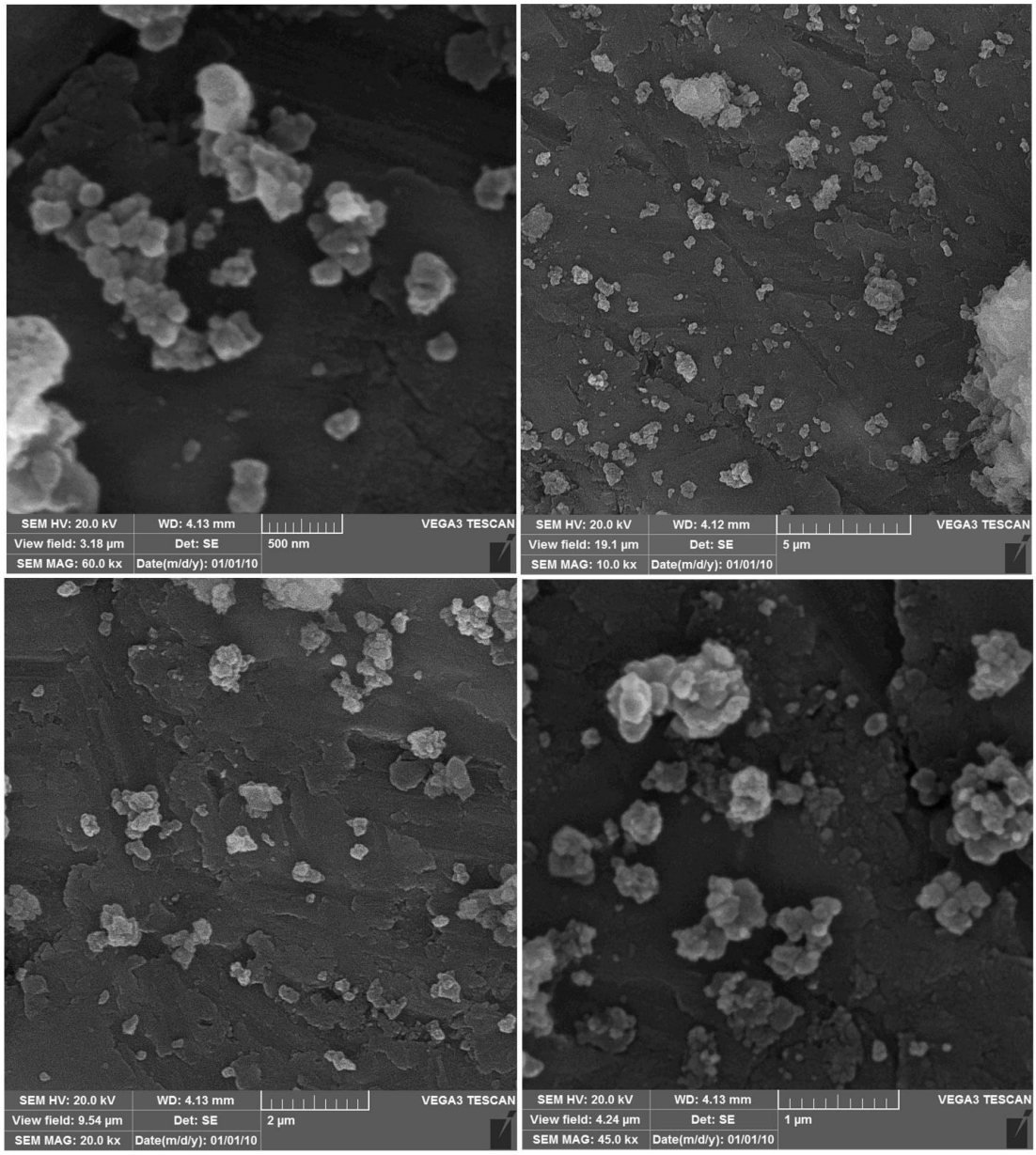

Fig. 3. FESEM images of the as-prepared materials of GO-Fe_3O_4/WO_3 nanocomposite

of atomic magnetic moments on the surface of nanoparticles. The saturation magnetization of GO-Fe_3O_4@WO_3 is equal to 26.4 emu g^{-1}, which is lower than that of the graphene oxide nanoparticles. These results show that the magnetization of GO-Fe_3O_4/WO_3 nanocomposite is lower than that of GO-Fe_3O_4, which can be attributed to the GO-Fe_3O_4/WO_3 surfaces being covered by tungsten trioxide particles that are not magnetically active. In these cases, applying an external magnetic field can ensure easy separation of GO-Fe_3O_4/WO_3 magnetization from the reaction medium.

Field emission scanning electron microscope (*FE-SEM)*

Morphological analysis and particle size of the synthesized nanocomposite were studied by scanning electron microscopy [40]. In Fig. 3, the morphologies and characteristics of GO-Fe_3O_4/WO_3 nanocomposite can be observed via FE-SEM images with different magnifications. As can be seen, the FE-SEM images show a rough surface

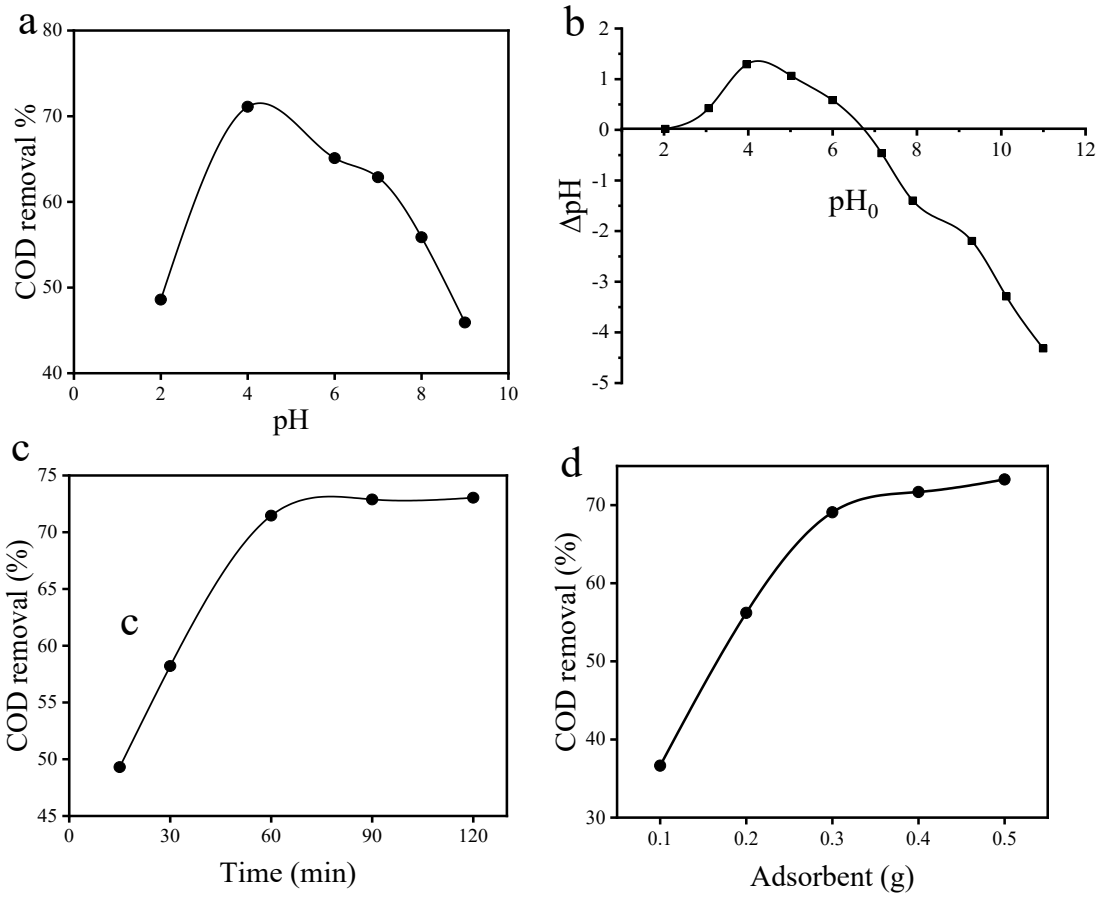

Fig. 4. (a) Effect of pH (b) pH_{pzc} (c) contact time and (d) Effect of dosage on the adsorption capacity.

in the GO-Fe_3O_4/WO_3 material with a good distribution of Fe_3O_4 and WO_3 nanoparticles on the GO sheets. Based on Fig. 2d, the average size of coated nanoparticles on graphene oxide nanosheets is 28.36 nm. These results indicate that the nanocomposite structure has been successfully formed.

Effects of initial pH

The initial pH of the solution is one of the most important controlling parameters in the adsorption process [45]. The effect of initial pH values on the sorption of COD ions by the adsorbent in the pH range of 2 to 8 is illustrated in Fig. 4a. As can be seen, the highest amount of removal is at a pH equal to 5, and the adsorption percentage decreases with a further increase in pH. While the highest removal efficiency was observed at pH 5, little difference was observed in COD removal at pH 6 and 7. This can be due to the alkalinity of the leachate environment and the positive surface of the nanocomposite synthesized with the graphene oxide substrate, the surface absorption is low, and when the pH of the leachate decreases. Electrostatic attraction between the magnetic nanocomposite and the pollutants in the leachate is created and higher COD removal is observed [46]. Also, due to the destruction of iron (III) oxide structure in highly acidic environments, the removal efficiency decreases at lower pH values [47].

The dependence of the chemical and electronic properties of functional groups on the surface of materials is related to the point of zero charge (pH_{pzc}). Fig. 4b presents the results of pHpzc determination. According to this figure, the GO-Fe_3O_4/WO_3 nanocomposite has a pH_{pzc} value of approximately 6.8. Consequently, at pH values above this threshold, the adsorbent surface carries a negative charge, whereas, at pH levels below this value, the adsorbent surface becomes positively charged.

Table. 2. Nonlinear kinetic model parameters for COD ions adsorption onto GO-Fe_3O_4/WO_3 magnetic nanocomposite

model	Parameter	Value
Pseudo-first-order	q_e (mg/g)	3006.81
	K_1 (min-1)	0.069
	R^2	0.95
Pseudo-second-order	q_e (mg/g)	3336.82
	K_2 (g/(mg.min))	3.14
	R^2	0.97
Intraparticle model	K_{id}	141.96
	C_i	1645.66
	R^2	0.82

Effects of the contact time

The influence of the contact time of the analyte and adsorbent is one of the basic parameters in studying the adsorption process evaluating the ability of adsorbents and comparing them with each other. Certainly, achieving the optimal adsorption capacity in the shortest period and establishing balance are among the distinctive features of a valuable adsorbent. Fig. 4c clearly shows that the adsorption is fast in the first 60 min and becomes slower with time and finally, the adsorbent is saturated. After that, with the increase of the contact time, no significant change was observed in the absorbent capacity, and in fact, equilibrium conditions were established. This could be because, in the early stages, many surface sites are available for pollutant adsorption, but with time, the remaining adsorption surface sites are hardly occupied due to the repulsion between the solute molecules and the solid phase [48]. In this case, pollutant adsorption penetrates from the surface sites to the internal sites of the absorber. These results have been observed and confirmed in the studies conducted by Ansari et al [49] and Soubh et al [50], which confirm that an increase in contact time has a positive effect on increasing the removal efficiency by enhancing the interaction between the pollutant and the absorbent.

The effects of adsorbent dosage

The effect of adsorbent dosage used in the COD removal process is an important factor in determining the adsorption capacity of the adsorbent in purification processes. As can be seen in Fig. 4d, increasing the adsorbent dosage has increased COD removal due to the increase in surface area and the availability of adsorption sites. However, with a further increase in the adsorbent dosage, pollutant adsorption remains almost constant. Liu et al. [51] studied the activated carbon adsorbent modified with Fe_3O_4 nanoparticles and found that increasing the adsorbent amount increased the removal efficiency due to the increased contact surface and the presence of more sites. Therefore, based on the obtained results, a fixed amount of 0.40 g of the adsorbent dosage was considered the optimal amount to maintain high absorption capacity with a COD removal efficiency of about 71% and provide a better comparison.

Adsorption kinetic

The results of the kinetic studies on the adsorption process provide significant information regarding the pathway, mechanism, and speed of the absorption process [52]. The adsorption kinetic process in this study was conducted using pseudo-first-order, pseudo-second-order, and intraparticle kinetic models. Fig. 5 indicates the kinetics of COD adsorption from leachate by GO-Fe3O4/WO3 nanocomposite. The fitting of kinetic data and parameter values related to pseudo-first-order, pseudo-second-order, and intraparticle kinetic models is presented in Table 2. According to the kinetic modeling data, it can be seen in Table 1 that COD adsorption on the GO-Fe_3O_4/WO_3 surface is in high agreement with the pseudo-second-order model with a correlation coefficient (R^2=0.97) compared to the pseudo-first-order model (R^2=0.95) and intraparticle kinetic model (R^2=82). Therefore, these results indicate that chemisorption can be the most dominant mechanism of the adsorption process involving valence forces through electron exchange between nanocomposite adsorption sites and leachate compounds [53].

Adsorption isotherms

Isotherm studies were conducted using the adsorbent nanocomposite GO-Fe3O4/WO3 for

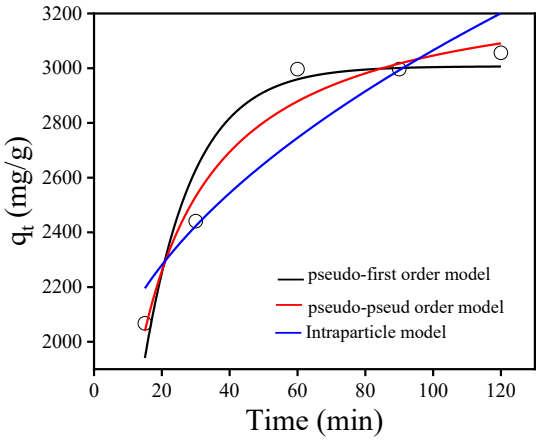

Fig. 5. Fitting of nonlinear kinetic models for kinetic adsorption studies using GO-Fe_3O_4 /WO_3 magnetic nanocomposite.

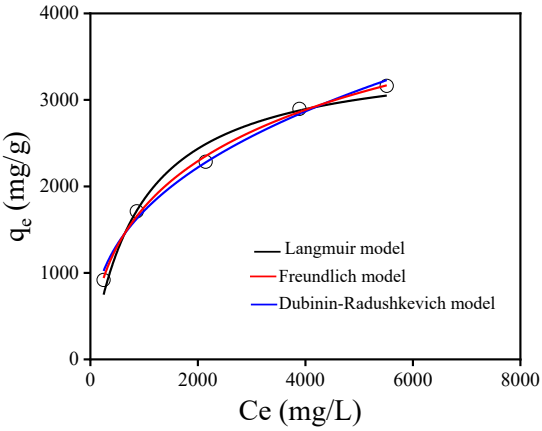

Fig. 6. Fitting of nonlinear Langmuir, Freundlich, and Dubinin-Radushkevich isotherm models for COD ions adsorption by GO-Fe_3O_4/WO_3 magnetic nanocomposite.

Table. 3. Nonlinear Langmuir, Freundlich, and Dubinin-Radushkevich isotherm model parameters and correlation coefficients for the adsorption of COD ions onto GO-Fe_3O_4/WO_3 magnetic nanocomposite.

model	Parameter	Value
Langmuir	q_m (mg/g)	3561.83
	K_L (L/mg)	0.011
	R^2	0.975
Freundlich	K_F (mg/g (L/mg))(1/n)	0.396
	n	3.14
	R^2	0.997
Dubinin-Radushkevich	qs (mg/g)	6277.56
	K_{ad} (mol^2/J^2)	0.0079
	R^2	0.987

COD adsorption at a temperature of 25°C. Fig. 6 illustrates the equilibrium adsorbed amount of COD (q_e) vs. the equilibrium COD concentration (C_e), along with the fitting results obtained from the nonlinear Langmuir, Freundlich, and Dubinin-Radushkevich models. The parameter values for both models are presented in Table 3. Based on the correlation coefficient, it can be concluded that the GO-Fe_3O_4/WO_3 nanocomposite follows the Freundlich isotherm model, suggesting a heterogeneous and multilayered adsorption process [54]. Additionally, the Langmuir model calculated a maximum adsorption capacity of 3561.83 mg/g, indicating a dominant exothermic process. The RL value determines the favorability of the adsorption isotherm shape, with RL > 1 indicating unfavorable, RL = 1 indicating linear, 0<RL<1 indicating favorable, and RL = 0 indicating irreversible [55]. In the case of COD adsorption on the nanocomposite, the RL value falls within the range of 0<RL<1, indicating a favorable adsorption process [56].

Adsorption thermodynamics

Temperature is usually considered a crucial parameter in sorption reactions. The effect of temperature in determining thermodynamic parameters such as the Entropy change: ΔS°, Enthalpy change: ΔH° and Gibbs free energy change: ΔG° was studied in the temperature range of 298 K to 358 K according to the Van Hoff equation. Thermodynamic parameters for COD ion adsorption using GO-Fe_3O_4/WO_3 were evaluated to demarcate the nature of the pollutant by Equations (10) and (11):

$$\Delta G^0 = -RT\ In\ K_R \tag{10}$$

$$In\ K_R = \frac{\Delta S^0}{R} - \frac{\Delta H^0}{RT} \tag{11}$$

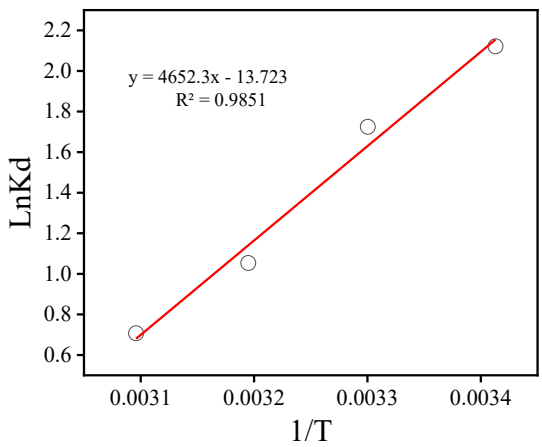

Fig. 7. Thermodynamic model for COD ions adsorption by GO-Fe_3O_4/WO_3 magnetic nanocomposite adsorbent.

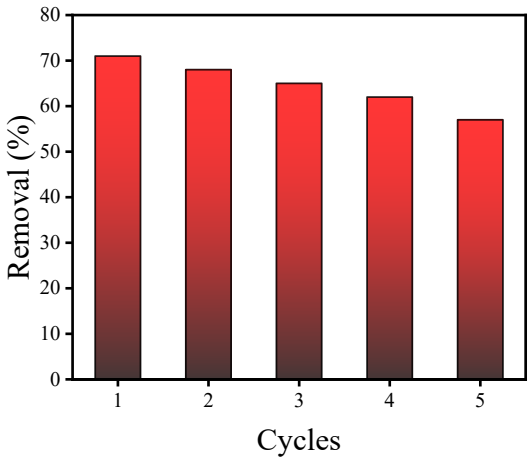

Fig. 8. Reusability assessment of GO-Fe_3O_4/WO_3 magnetic nanocomposite after the removal of COD ions.

Table. 4. Dynamic model parameters used in the adsorption process COD by GO-Fe_3O_4/WO_3 magnetic nanocomposite adsorbent.

T (°K)	LnKd	ΔG° ($KJmol^{-1}$)	ΔH° ($KJmol^{-1}$)	ΔS° ($KJmol^{-1}$)
298	2.122	-5.168	38.6792	114.093
303	1.725	-4.345		
313	1.053	-2.741		
323	0.707	-1.898		

Where K_R is the equilibrium constant; R is the gas constant, (8.314 J $K^{-1}mol^{-1}$), and T is the temperature on the Kelvin scale (298 K). The corresponding values of ΔS°, ΔH°, and ΔG° were calculated according to the fitting data, and the results are presented in Table 3.

The influence of the adsorption temperature on the adsorption capacity of COD ions onto the adsorbent has been displayed by a linear plot of lnKd versus 1/T in Fig. 7, and the values of the thermodynamic parameters are listed in Table 4. As the results show, the value of ΔG° is negative at all set temperature conditions, the reaction is therefore spontaneous (ΔG° < 0). Moreover, a negative value of the enthalpy change of ΔH°< 0 illustrates the exothermic nature of the adsorption process. The value of ΔH° is less than 100 kJ mol-1, thus indicating that the temperature has little effect on the reaction of the adsorption process and the interaction between GO-Fe_3O_4/WO_3 and COD is not strong. Consequently, the negative values of ΔS° demonstrate that no significant change in entropy occurred during adsorption because the increase in entropy of the system causes the release of ions from the solid surface to the solution [57]. On the other hand, the release of water molecules produced by the interaction of COD ions with the functional groups and surface sites of the adsorbent resulted in a positive ΔS° value [58].

Regeneration Capability

That adsorbent can be regenerated or consumed several times is an important factor in determining whether the adsorbent can be widely used. Therefore, the HCl solution (0.1 M) was used as a regenerator to regenerate the adsorbent after reaching the adsorption equilibrium. As can be seen from the results of Fig. 8, the adsorption capacity of GO-Fe_3O_4/WO_3 was about 57% after five cycles. The regeneration results revealed that the adsorbent has good stability and high COD absorption capacity after five stages. These results revealed that the adsorbent has a high potential for application in the removal of COD ions from landfill leachates.

CONCLUSION

In this study, a new magnetic graphene oxide adsorbent WO_3 was successfully prepared by a safe and simple hydrothermal method for COD removal from landfill leachate. The results of this adsorption study showed that GO-Fe_3O_4/

WO_3 is an effective adsorbent for COD removal from landfill leachates. The adsorption process of COD reached equilibrium at optimum pH 4, 90 min, the adsorbent dosage of 25 mg/g, and below 293 K. The experimental adsorption data were found to follow the adsorption kinetics from the pseudo-second-order model and the Freundlich isotherm equation, indicating that chemisorption is the rate-determining step. The maximum multilayered adsorption capacity of COD from the leachate by the adsorbent is found to be 3561.83 mg/g. The thermodynamic model shows that the adsorption of COD by the adsorbent is exothermic and spontaneous. In conclusion, the results showed that GO-Fe_3O_4/WO_3 sorbent can be used as a potential adsorbent for the adsorption of contamination from landfill leachates.

CONFLICT OF INTEREST

The authors hereby declare that there is no conflict of interest.

REFERENCES

[1] Sayadi, M.; Rezaei, M.; Rezaei, A., Fraction distribution and bioavailability of sediment heavy metals in the environment surrounding MSW landfill: a case study, Environmental monitoring and assessment, 2015, 187, 1-11, , https://doi.org/10.1007/s10661-014-4110-1.

[2] Erabee, I.; Ahsan, A.; Jose, B.; Aziz, M.; Ng, A.; Idrus, S.; et al., Adsorptive treatment of landfill leachate using activated carbon modified with three different methods, KSCE Journal of Civil Engineering, 2018, 22, 1083-95, https://doi.org/10.1007/s12205-017-1430-z.

[3] Mojiri, A.; Zhou, J.L.; Ratnaweera, H.; Ohashi, A.; Ozaki, N.; Kindaichi, T.; et al., Treatment of landfill leachate with different techniques: an overview, Journal of Water Reuse and Desalination, 2021, 11, 66-96, https://doi.org/10.2166/wrd.2020.079.

[4] Reshadi, M.A.M.; Bazargan, A.; McKay, G., A review of the application of adsorbents for landfill leachate treatment: Focus on magnetic adsorption. Science of the total environment, 2020, 731, 138863, https://doi.org/10.1016/j.scitotenv.2020.138863

[5] Abdel-Shafy, H.I.; Ibrahim, A.M.; Al-Sulaiman, A.M.; Okasha, R.A., Landfill leachate: Sources, nature, organic composition, and treatment: An environmental overview, Ain Shams Engineering Journal, 2023, 102293, https://doi.org/10.1016/j.asej.2023.102293

[6] Shokri, A.; Salimi, M.; Abmatin, T., Employing photo Fenton and UV/ZnO processes for removing Reactive red 195 from aqueous environment, Fresenius Environmental Bulletin, 2017, 26, 1560-5.

[7] Naveen, B.; Mahapatra, D.M.; Sitharam, T.; Sivapullaiah, P.; Ramachandra, T., Physico-chemical and biological characterization of urban municipal landfill leachate, Environmental Pollution, 2017, 220, 1-12, https://doi.org/10.1016/j.envpol.2016.09.002

[8] Lim, C.K.; Seow, T.W.; Neoh, C.H.; Md Nor, M.H.; Ibrahim, Z.; Ware, I.; et al, Treatment of landfill leachate using ASBR combined with zeolite adsorption technology, 3 Biotech, 2016, 6, 1-6, https://doi.org/10.1007/s13205-016-0513-8.

[9] Bashir, M.J.; Xian, T.M.; Shehzad, A.; Sethupahi, S.; Choon Aun, N.; Abu Amr, S, Sequential treatment for landfill leachate by applying coagulation-adsorption process, Geosystem engineering, 2017, 20, 9-20, https://doi.org/10.1080/12269328.2016.1217798.

[10] Dolar, D.; Košutić, K.; Strmecky, T, Hybrid processes for treatment of landfill leachate: coagulation/UF/NF-RO and adsorption/UF/NF-RO, Separation and Purification Technology, 2016, 168, 39-46, https://doi.org/10.1016/j.seppur.2016.05.016.

[11] Wang, Z.; Huang, Y.; Yang, J.; Li, Y.; Zhuang, Q.; Gu, J, The water-based synthesis of chemically stable Zr-based MOFs using pyridine-containing ligands and their exceptionally high adsorption capacity for iodine, Dalton Transactions, 2017, 46, 7412-20, https://doi.org/ 10.1039/C7DT01084B.

[12] Zheng, H.; Gao, Y.; Zhu, K.; Wang, Q.; Wakeel, M.; Wahid, A.; et al, Investigation of the adsorption mechanisms of Pb (II) and 1-naphthol by β-cyclodextrin modified graphene oxide nanosheets from aqueous solution, Journal of colloid and interface science, 2018, 530, 154-62, https://doi.org/10.1016/j.jcis.2018.06.083

[13] Yao, X.; Yan, Z.; Wang, X.; Jiang, H.; Qian, Y.; Fan, C, The influence of reduced graphene oxide on stem cells: a perspective in peripheral nerve regeneration, Regenerative Biomaterials, 2021, 8, rbab032, https://doi.org/10.1093/rb/rbab032.

[14] Sontakke, A.D.; Purkait, M.K, A brief review on graphene oxide nanoscrolls: structure, synthesis, characterization and scope of applications, Chemical Engineering Journal, 2021, 420, 129914, https://doi.org/10.1016/j.cej.2021.129914.

[15] El-Shafai, N.M.; Abdelfatah, M.M.; El-Khouly, M.E.; El-Mehasseb, I.M.; El-Shaer, A.; Ramadan, M.S.; et al, Magnetite nano-spherical quantum dots decorated graphene oxide nano sheet (GO@ Fe_3O_4): electrochemical properties and applications for removal heavy metals, pesticide and solar cell, Applied Surface Science, 2020, 506, 144896, , https://doi.org/10.1016/j.apsusc.2019.144896

[16] Rajabi, M.; Mahanpoor, K.; Moradi, O, Preparation of PMMA/GO and PMMA/GO-Fe_3O_4 nanocomposites for malachite green dye adsorption: kinetic and thermodynamic studies, Composites Part B: Engineering, 2019, 167, 544-55, https://doi.org/10.1016/j.compositesb.2019.03.030

[17] Koushkbaghi, S.; Jafari, P.; Rabiei, J.; Irani, M.; Aliabadi, M, Fabrication of PET/PAN/GO/Fe_3O_4 nanofibrous membrane for the removal of Pb (II) and Cr (VI) ions, Chemical Engineering Journal, 2016, 301, 42-50, https://doi.org/10.1016/j.cej.2016.04.076

[18] Ahmadifar, Z.; Dadvand Koohi, A, Characterization, preparation, and uses of nanomagnetic Fe 3 O 4 impregnated onto fish scale as more efficient adsorbent for Cu^{2+} ion adsorption, Environmental Science and Pollution Research, 2018, 25, 19687-700, https://doi.org/10.1007/s11356-018-2058-3

[19] Wang, Y.; Wu, X.; Zhang, W.; Luo, C.; Li, J.; Wang, Q, 3D heterostructure of graphene@ Fe_3O_4@WO_3@PANI: Preparation and excellent microwave absorption performance, Synthetic Metals, 2017, 231, 7-14, https://doi.org/10.1016/j.synthmet.2017.06.013

[20] Sayadi, M.H.; Ahmadpour, N., Homaeigohar, S; Photocatalytic and antibacterial properties of Ag-$CuFe_2O_4$@

WO_3 magnetic nanocomposite, Nanomaterials, 2021, 11, 298, https://doi.org/10.3390/nano11020298

[21] Peleyeju, M.G.; Viljoen, E.L, WO3-based catalysts for photocatalytic and photoelectrocatalytic removal of organic pollutants from water–A review, Journal of Water Process Engineering, 2021, 40, 101930, https://doi.org/10.1016/j.jwpe.2021.101930

[22] Moghazy, M.A, Leidenfrost green synthesis method for MoO_3 and WO_3 nanorods preparation: characterization and methylene blue adsorption ability, BMC chemistry, 2023, 17, 1-11, https://doi.org/10.1186/s13065-023-00916-3

[23] Feng, X.; Li, X.; Su, B.; Ma, J, Two-step construction of WO_3@TiO_2/CS-biochar S-scheme heterojunction and its synergic adsorption/photocatalytic removal performance for organic dye and antibiotic, Diamond and Related Materials, 2023, 131, 109560, https://doi.org/10.1016/j.diamond.2022.109560

[24] Rashki, O.; Rezaei, M.R.; Sayadi, M.H, The high photocatalytic efficiency and stability of the Z-scheme $CaTiO_3/WS_2$ heterostructure for photocatalytic removal of 17α-ethinyl estradiol in aqueous solution, Journal of Photochemistry and Photobiology A: Chemistry, 2022, 433, 114169, https://doi.org/10.1016/j.jphotochem.2022.114169

[25] Bankole, M.T.; Abdulkareem, A.S.; Tijani, J.O.; Ochigbo, S.S.; Afolabi, A.S.; Roos, W.D, Chemical oxygen demand removal from electroplating wastewater by purified and polymer functionalized carbon nanotubes adsorbents, Water Resources and Industry, 2017, 18, 33-50, https://doi.org/10.1016/j.wri.2017.07.001

[26] Gholami, P.; Khataee, A.; Vahid, B, Integration of Polydopamine and Fe_3O_4 Nanoparticles with Graphene Oxide to Fabricate an Efficient Recoverable Catalyst for the Degradation of Sulfadiazine, Industrial & Engineering Chemistry Research, 2020, 59, 183-93, https://doi.org/10.1021/acs.iecr.9b05130

[27] Lam, S.-M.; Sin, J.-C.; Lin, H.; Li, H.; Lim, J.W.; Zeng, H, A Z-scheme WO_3 loaded-hexagonal rod-like ZnO/Zn photocatalytic fuel cell for chemical energy recuperation from food wastewater treatment, Applied Surface Science, 2020, 514, 145945, https://doi.org/10.1016/j.apsusc.2020.145945

[28] Rezaei, A.; Rezaei; M.R.; Sayadi, M.H, Enhanced 3, 5-dimethylphenol photodegradation via adsorption-photocatalysis synergy using FSTRG nanohybrid catalyst, Journal of Molecular Liquids, 2021, 335, 116546, https://doi.org/10.1016/j.molliq.2021.116546

[29] Chen, W.-H.; Huang, J.-R.; Lin, C.-H.; Huang, C.-P, Catalytic degradation of chlorpheniramine over GO-Fe_3O_4 in the presence of H_2O_2 in water: The synergistic effect of adsorption, Science of The Total Environment, 2020, 736, 139468, https://doi.org/10.1016/j.scitotenv.2020.139468

[30] Yao, S.; Qu, F.; Wang, G.; Wu, X, Facile hydrothermal synthesis of WO_3 nanorods for photocatalysts and supercapacitors, Journal of Alloys and Compounds, 2017, 724, 695-702, https://doi.org/10.1016/j.jallcom.2017.07.123

[31] Zadeh, R.J.; Sayadi, M.H.; Rezaei, M.R, Synthesis of Thiol modified magMCM-41 nanoparticles with rice husk ash as a robust, high effective, and recycling magnetic sorbent for the removal of herbicides, Journal of Environmental Chemical Engineering, 2021, 9, 104804, https://doi.org/10.1016/j.jece.2020.104804

[32] Gohari, R.M.; Safarnia, M.; Koohi, A.D.; Salehi, M.B, Adsorptive removal of cationic dye by synthesized sustainable xanthan gum-g p (AMPS-co-AAm) hydrogel from aqueous media: Optimization by RSM-CCD model, Chemical Engineering Research and Design, 2022, 188, 714-28, https://doi.org/10.1016/j.cherd.2022.10.028

[33] Azin, A.; Koohi, A.D.; Padekan, B, Chitosan–collagen/hydroxyapatite and tripolyphosphate nanocomposite: characterization and application for copper removal from aqueous solution, Polymer Bulletin, 2022, 1-25, https://doi.org/10.1007/s00289-021-03998-y

[34] Rahmani, M.; Dadvand Koohi, A, Adsorption of malachite green on the modified montmorillonite/xanthan gum-sodium alginate hybrid nanocomposite, Polymer Bulletin, 2022, 79, 8241-67, https://doi.org/10.1007/s00289-021-03889-2

[35] Jalali, M.A.; Koohi, A.D.; Sheykhan, M, Experimental study of the removal of copper ions using hydrogels of xanthan, 2-acrylamido-2-methyl-1-propane sulfonic acid, montmorillonite: Kinetic and equilibrium study, Carbohydrate Polymers, 2016, 142, 124-32, https://doi.org/10.1016/j.carbpol.2016.01.033

[36] Rezaei, A.; Rezaei, M.R.; Sayadi, M.H, 3D network structure graphene hydrogel-Fe_3O_4@ SnO_2/Ag via an adsorption/photocatalysis synergy for removal of 2, 4 dichlorophenol, Journal of the Taiwan Institute of Chemical Engineers, 2021, 121, 154-67, https://doi.org/10.1016/j.jtice.2021.03.048

[37] Rocha, K.; Zanetti, S, Structural and properties of nanocrystalline WO_3/TiO_2-based humidity sensors elements prepared by high energy activation, Sensors and Actuators B: Chemical, 2011, 157, 654-61, https://doi.org/10.1016/j.snb.2011.05.048.

[38] Sarkar, C.; Nath, J.; Bhuyan, S.; Dolui, S.K, Multifunctional ternary nanocomposites of Ni/Polypyrrole/Reduced graphene oxide as supercapacitor and electrocatalyst in methanol oxidation, ChemistrySelect, 2019, 4, 2529-37. https://doi.org/10.1002/slct.201803386

[39] Sayadi, M.H.; Homaeigohar, S.; Rezaei, A.; Shekari, H, Bi/SnO_2/TiO_2-graphene nanocomposite photocatalyst for solar visible light–induced photodegradation of pentachlorophenol, Environmental Science and Pollution Research, 2021, 28, 15236-47, https://doi.org/10.1007/s11356-020-11708-w

[40] Shokri, A.; Mahanpoor, K, Removal of ortho-toluidine from industrial wastewater by UV/TiO_2 process, Journal of Chemical Health Risks, 2016, 6, 3, 213-223.

[41] Shokri, A.; Sanavi Fard, M, Using α-Fe_2O_3/SiO_2 as a heterogeneous Fenton catalyst for the removal of chlorophenol in aqueous environment: Thermodynamic and kinetic studies, International Journal of Environmental Science and Technology, 2023, 20, 383-96, https://doi.org/10.1007/s13762-022-04498-w

[42] Rajalakshmi, R.; Rebekah, A.; Viswanathan, C., Ponpandian, N. Evolution of intrinsic 1-3D WO_3 nanostructures: Tailoring their phase structure and morphology for robust hydrogen evolution reaction, Chemical Engineering Journal, 2022, 428, 132013, https://doi.org/10.1016/j.cej.2021.132013

[43] Daraie, M.; Heravi, M.M.; Kazemi, S.S, Pd@ GO/Fe_3O_4/PAA/DCA: a novel magnetic heterogeneous catalyst for promoting the Sonogashira cross-coupling reaction, Journal of Coordination Chemistry, 2019, 72, 2279-93, https://doi.org/10.1080/00958972.2019.1640360

[44] Esmaili, N.; Mohammadi, P.; Abbaszadeh, M.; Sheibani, H,

Green synthesis of silver nanoparticles using Eucalyptus comadulensis leaves extract and its immobilization on magnetic nanocomposite (GO-Fe_3O_4/PAA/Ag) as a recoverable catalyst for degradation of organic dyes in water, Applied Organometallic Chemistry, 2020, 34, e5547, https://doi.org/10.1002/aoc.5547

[45] Gamoudi, S.; Srasra, E, Adsorption of organic dyes by HDPy+-modified clay: effect of molecular structure on the adsorption, Journal of Molecular Structure, 2019, 1193, 522-31, https://doi.org/10.1016/j.molstruc.2019.05.055

[46] Shadi, A.M.H.; Kamaruddin, M.A.; Niza, N.M.; Emmanuel, M.I.; Hossain, M.S.; Ismail, N, Efficient treatment of raw leachate using magnetic ore iron oxide nanoparticles Fe_2O_3 as nanoadsorbents, Journal of Water Process Engineering, 2020, 38, 101637, https://doi.org/10.1016/j.jwpe.2020.101637

[47] Li, F.; Huang, T.; Sun, F.; Chen, L.; Li, P.; Shao, F.; et al, Ferric oxide nanoclusters with low-spin FeIII anchored g-C_3N_4 rod for boosting photocatalytic activity and degradation of diclofenac in water under solar light, Applied Catalysis B: Environmental, 2022, 317, 121725, https://doi.org/10.1016/j.apcatb.2022.121725

[48] Zhou, L.; Liang, Q.; Chai, K.; Tong, Z.; Ji, H, A cost-effective β-cyclodextrin polymer for selective adsorption and separation of acetophenone and 1-phenylethanol via specific noncovalent molecular interactions, Reactive and Functional Polymers, 2020, 146, 104448, https://doi.org/10.1016/j.reactfunctpolym.2019.104448

[49] Ansari, R.; Mosayebzadeh, Z, Application of polyaniline as an efficient and novel adsorbent for azo dyes removal from textile wastewaters, Chemical Papers, 2011, 65, 1-8, https://doi.org/10.2478/s11696-010-0083-x

[50] Soubh, A.M.; Baghdadi, M.; Abdoli, M.A.; Aminzadeh, B, Zero-valent iron nanofibers (ZVINFs) immobilized on the surface of reduced ultra-large graphene oxide (rULGO) as a persulfate activator for treatment of landfill leachate, Journal of environmental chemical engineering, 2018, 6, 6568-79, https://doi.org/10.1016/j.jece.2018.10.011

[51] Liu, X.; Tian, J.; Li, Y.; Sun, N.; Mi, S.; Xie, Y.; et al, Enhanced dyes adsorption from wastewater via Fe_3O_4 nanoparticles functionalized activated carbon, Journal of hazardous materials, 2019, 373, 397-407, https://doi.org/10.1016/j.jhazmat.2019.03.103

[52] Shakib, F.; Dadvand Koohi, A.; Kamran Pirzaman, A, Adsorption of methylene blue by using novel chitosan-g-itaconic acid/bentonite nanocomposite–equilibrium and kinetic study, Water Science and Technology, 2017, 75, 1932-43, https://doi.org/10.2166/wst.2017.077

[53] Tang, Y.; Alam, M.S.; Konhauser, K.O.; Alessi, D.S.; Xu, S.; Tian, W.; et al, Influence of pyrolysis temperature on production of digested sludge biochar and its application for ammonium removal from municipal wastewater, Journal of Cleaner Production, 2019, 209, 927-36, https://doi.org/10.1016/j.jclepro.2018.10.268

[54] Hadroug, S.; Jellali, S.; Azzaz, A.A.; Kwapinska, M.; Hamdi, H.; Leahy, J.J.; et al, Valorization of salt post-modified poultry manure biochars for phosphorus recovery from aqueous solutions: Investigations on adsorption properties and involved mechanism, Biomass Conversion and Biorefinery, 2022, 12, 4333-48, https://doi.org/10.1007/s13399-021-02099-0

[55] Pathak, P.D.; Mandavgane, S.A, Preparation and characterization of raw and carbon from banana peel by microwave activation: application in citric acid adsorption, Journal of Environmental Chemical Engineering, 2015, 3, 2435-47, https://doi.org/10.1016/j.jece.2015.08.023

[56] Fu, L.; Wang, R.; Zhao, C.; Huo, J.; He, C.; Kim, K.-H.; et al, Construction of Cr-embedded graphyne electrocatalyst for highly selective reduction of CO2 to CH4: A DFT study, Chemical Engineering Journal, 2021, 414, 128857, https://doi.org/10.1016/j.cej.2021.128857

[57] Qin, H.; Xiao, R.; Guo, L.; Meng, J.; Chen, J, Mercury (II) adsorption from aqueous solution using nitrogen and sulfur co-doped activated carbon, Water Science and Technology, 2018, 2017, 310-8, https://doi.org/10.2166/wst.2018.117

[58] Deb, A.S.; Dwivedi, V.; Dasgupta, K.; Ali, S.M.; Shenoy, K, Novel amidoamine functionalized multi-walled carbon nanotubes for removal of mercury (II) ions from wastewater: combined experimental and density functional theoretical approach, Chemical Engineering Journal, 2017, 313, 899-911, https://doi.org/10.1016/j.cej.2016.10.126